

# A High-Efficiency Active Battery-Balancing Circuit Using Multiwinding Transformer

Siqi Li, Chunting Chris Mi, *Fellow, IEEE*, and Mengyang Zhang, *Member, IEEE*

**Abstract**—This paper presents a simple circuit for balancing series-connected battery cells. The circuit is composed of one low-voltage metal–oxide–semiconductor field-effect transistor (MOSFET) for each cell and a symmetrical multiwinding transformer for a group of cells. Only one control signal is needed for all MOSFETs, and energy can be directly transferred from higher voltage cells to lower voltage cells. A small capacitor is added to form a resonant circuit with the transformer magnetizing inductance so that soft switching can be achieved in some operation range to obtain high efficiency. The circuit balance function and soft-switching condition are analyzed and verified by simulation and experiments. A circuit for balancing a 4- and 12-cell battery group is tested. The experimental results showed the effectiveness of the circuit. The energy transfer efficiency between cells can reach up to 93%. The circuit can be easily scaled to battery strings containing up to 12 battery cells, directly applicable to consumer electronics application where the number of cells is typically less than 12. A battery pack containing a large number of battery cells, such as the ones used in electric vehicles, can be balanced in groups, for example, in modules containing 12 cells each and with one additional circuit to balance among the modules.

**Index Terms**—Batteries, battery balancing, electric vehicle, multiwinding transformer, plug-in hybrid electric vehicle, soft-switching.

## I. INTRODUCTION

**D**UE TO CONCERNS over energy security and the environment, plug-in hybrid electric vehicles (EV) (PHEVs) and pure EVs have become the research hot spot recently. In EV and PHEV, a high-power traction battery plays an important role. Lithium-ion batteries are preferred in EVs and PHEVs for their superior power and energy density. On the other hand, lithium-ion batteries have been dominating the consumer electronics products, such as laptops and cellular phones. Unlike lead–acid batteries, lithium-ion batteries are highly intolerant to overcharging, and their safety is of top concern due to overcharge, overdischarge, and improper use.

Manuscript received February 27, 2012; revised May 7, 2012; accepted May 8, 2012. Date of publication November 21, 2012; date of current version January 16, 2013. Paper 2012-TSC-102.R1, presented at the 2012 IEEE Applied Power Electronics Conference and Exposition, Orlando, FL, February 5–9, and approved for publication in the IEEE TRANSACTIONS ON INDUSTRY APPLICATIONS by the Transportation Systems Committee of the IEEE Industry Applications Society. This work was supported by the U.S. Department of Energy under Grant DOE DE-EE0002720.

S. Li and C. C. Mi are with the Department of Electrical and Computer Engineering, University of Michigan, Dearborn, MI 48128 USA (e-mail: lisiqi00@gmail.com; chrismi@umich.edu).

M. Zhang is with Electrified Propulsion Systems, Chrysler Group LLC, Auburn Hills, MI 48321-8004 USA (e-mail: mz91@chrysler.com).

Color versions of one or more of the figures in this paper are available online at <http://ieeexplore.ieee.org>.

Digital Object Identifier 10.1109/TIA.2012.2229455

A battery management system (BMS) with a balance function is always necessary when a large number of lithium-ion battery cells are connected in series for high-power and high-energy applications. The balance function is very important for the health, safety, available capacity, and life of the series-connected battery cells [1]–[4].

The balance circuits can be classified into two types: One uses energy dissipation method, and the other uses energy recovery method. The energy dissipation method dissipates the excess energy of higher voltage cells on a resistor or transistor [5], [6]. The balance current is limited by heat dissipation of the battery pack. Specifically speaking, all the excess energy is dissipated in the resistor or transistor as heat, so the balance efficiency is zero. This kind of balance circuit has already been used in many applications for its simple structure and reliability. The other method, the energy recovery method, transfers the excess energy among cells or between cells and the pack; hence, more efficient and rapid balancing can be expected.

To realize energy recovery, it is common to introduce an individual cell equalizer (equalizer, for short) for each cell [7]–[14]. One kind of cell equalizer can exchange energy between arbitrary cells [13] or between cells and the pack [14]. The circuit and its control strategy of this type of cell equalizer are complicated. To mitigate the complexity, equalizers with the ability to exchange energy only between adjacent cells are proposed in many papers [7]–[11]. For this type of balancing topology, there is no need for isolation, and only low-voltage power devices are needed. Usually, the circuit for each battery cell is simple, and high efficiency can be achieved when energy transfers between adjacent cells. However, as the number of the battery cells in a battery string grows, the efficiency could decrease quickly. References [9] and [10] present a well-designed quasi-resonant zero-current-switching bidirectional converter for the battery equalization. The claimed energy transfer efficiency is 85% maximum in a three-cell series-connected battery string. If the string grows to five cells, the energy from one end to another end has to pass four stages, so the efficiency will most likely drop to below 70%. With a longer battery string, more energy will be lost on the transfer path.

Another way of energy recovery balancing is using a multiwinding transformer [2], [15]–[19]. A group of battery cells are coupled by the multiwinding transformer, so energy can be exchanged between arbitrary cells in a group. Therefore, high efficiency can be expected. By introducing a symmetrical multiwinding transformer, the battery voltage can be equalized autonomously, so the control logic can be simplified [2], [17]–[19]. With the symmetrical multiwinding transformer, it is not desirable to involve the diode voltage drop. One reason is that

the diode voltage drop is about 10%–20% of the cell voltage; hence, a significant portion of the transferred energy will be lost. Another reason is that the voltage drop distribution and temperature coefficient may cause variance of the final cell voltages.

The main disadvantage of using a multiwinding transformer is that it is hard to make a transformer with several tens or hundreds of windings. However, this can be overcome by modularization [19], [20]. Cells are divided into groups. First, cells are balanced inside a group, and then, the groups are balanced by a second stage circuit. The other problem of using a symmetrical multiwinding transformer is that it can only balance the voltage between each cell. When the lithium-ion battery is in the middle charged status, the voltage difference is very small if the state of charge (SOC) only has a few percent of differences.

The best way to balance a battery string is to calculate the SOC of each cell and control the balance current to equalize the SOC [14]. However, obtaining accurate SOC of each individual cell is very difficult or even impractical problem. Simply balancing by voltage is commonly adopted, and the results are acceptable [2], [6], [8]–[12].

This paper studies a high-efficiency direct balance circuit using a multiwinding transformer. Similar topologies have been proposed in [18]. In the proposed circuit, energy transfers from higher voltage cells to lower voltage cells directly. The balance results only rely on the symmetry of the transformer, so the implementation is potentially simpler than the existing balancing circuits. Accurate balancing, low cost, high efficiency, simple control, and ease of implementation are the main advantages of the battery-cell-balancing method proposed in this paper.

## II. BALANCE CIRCUIT TOPOLOGY

The balance circuit under study is shown in Fig. 1. For each battery cell, the same circuit parameter is applied. Take cell  $B_1$  for example,  $L_{f1}$  and  $C_{f1}$  are the inductor and capacitor of the output filter.  $C_{s1}$  forms an LC circuit with the transformer magnetic inductance; thus, the magnetization current can be reset, and soft switching can be achieved by resonance.  $T_{m1}$  is one winding of the multiwinding transformer. The balance circuit can support multicells by using a 1 : 1 : ... : 1 symmetrical multiwinding transformer. A switching device, typically metal–oxide–semiconductor field-effect transistor (MOSFET), is inserted between each battery cell and one winding of the transformer. When MOSFETs  $M_1, M_2, \dots, M_n$  are turned on and off, the battery cells will be coupled by the multiwinding transformer, and the voltage on each winding will be identical. When the MOSFETs are turned on, for higher voltage cells, the voltage on the battery side is higher than that on the winding side. So, energy will flow out of this cell and go into the transformer. For lower voltage cells, the voltage on the battery side is lower than that on the winding side. So, energy will flow into the cell from the transformer winding. The energy transfers from higher voltage cells to lower voltage cells directly.

Another multiwinding transformer can be used to drive the MOSFETs for gate isolation. Alternatively, a voltage level shift circuit can be applied to get rid of the driving multitransformer,

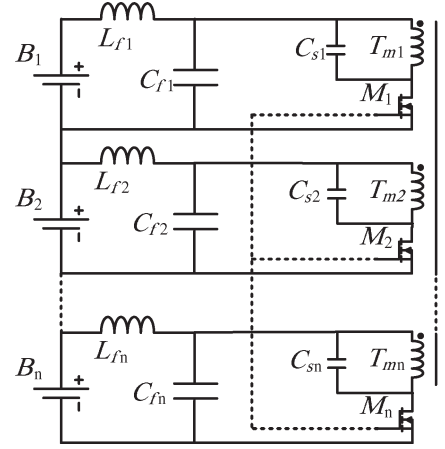


Fig. 1. Topology of the proposed balance circuit.

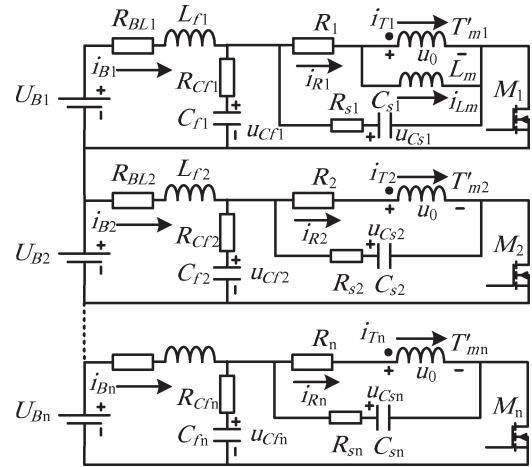


Fig. 2. Equivalent circuit model of the proposed balance circuit with parasitic resistance, named as Model A.

because the potential of all the MOSFETs' source terminals is fixed by the battery poles. With both approaches, all the MOSFETs will be driven by only one isolated primary side signal.

## III. CIRCUIT OPERATION PRINCIPLE

The balance circuit shown in Fig. 1 can be seen as a multiwinding forward converter. Fig. 2 shows its circuit model considering parasitic resistance, named as Model A. Stray inductance and capacitance are neglected for their relative small value compared with the circuit lumped parameters. Based on the model shown in Fig. 2, the balance function and magnetizing current reset of the circuit can be analyzed. To represent components related with a nonspecific battery cell in Fig. 1, subscript  $i$  ( $i = 1, 2, \dots, n$ ) is used to represent cell  $i$  in the battery string.

### A. Balance Function

The balance function mainly works when all the MOSFETs are in on-status. Neglecting the current on the snubber components and assuming that the output filter  $L_{fi}$  and  $C_{fi}$  are large enough, therefore, current  $i_{Bi}$  and voltage  $u_{Cfi}$  are almost

constant. However, the derivatives of  $i_{Bi}$  and  $u_{Cfi}$  are not zero. When the MOSFETs are on, the following relationships can be obtained:

$$u_{Cfi} + (i_{Bi} - i_{Ri}) \cdot R_{Cfi} = U_{Bi} - i_{Bi} \cdot R_{BLi} - L_{fi} \cdot \left( \frac{di_{Bi}}{dt} \right)_1 \quad (1)$$

$$u_{Cfi} = u_0 + (i_{Ri} - i_{Bi}) \cdot R_{Cfi} + i_{Ri} \cdot (R_i + R_{oni}) \quad (2)$$

where  $R_{BLi}$  is the overall resistance on the battery side,  $R_{oni}$  is the on-resistance of MOSFET  $M_i$ , and  $(di_{Bi}/dt)_1$  is the derivative of  $i_{Bi}$  during MOSFET on-period.

In (2), the soft switching is assumed such that the MOSFETs are turned on at zero voltage. So, before we turn on the MOSFETs, the voltage on snubber capacitor  $C_{si}$  is zero. Moreover, in the MOSFET on-period, the voltage on  $C_{si}$  is also zero. There is no current on  $C_{si}$  when the MOSFETs are on. When soft switching is not achieved, at the beginning of MOSFET turning on, the snubber current will bring some error. However, since capacitor  $C_{si}$  is very small, thus, (2) still has enough accuracy.

When the MOSFETs are off, the following equation can be obtained:

$$u_{Cfi} + i_{Bi} \cdot R_{Cfi} = U_{Bi} - i_{Bi} \cdot R_{BLi} - L_{fi} \cdot \left( \frac{di_{Bi}}{dt} \right)_2 \quad (3)$$

where  $R_{Cfi}$  is the equivalent series resistance of  $C_{fi}$  and  $(di_{Bi}/dt)_2$  is the derivative of  $i_{Bi}$  during MOSFET off period.

When the MOSFETs are off, the magnetization current  $i_{Lm}$  will resonate with  $C_s$ . The resonant characteristics are complex and vary with the on and off times. It can slightly affect the battery cell current  $i_{Bi}$ . The detail will be discussed later; here, we just consider  $i_{Ri}$  as zero during MOSFET off period for simplicity, and the following relationship can be obtained:

$$i_{Bi} = d \cdot i_{Ri\_on} \quad (4)$$

where  $i_{Ri\_on}$  is the current of  $R_i$  during MOSFET on-period derived from (2) and  $d$  is the MOSFET turn-on duty ratio.

Also, in one switching period, the current change on inductor  $L_{fi}$  should be zero; hence, we can get

$$\left( \frac{di_{Bi}}{dt} \right)_1 \cdot d + \left( \frac{di_{Bi}}{dt} \right)_2 \cdot (1 - d) = 0. \quad (5)$$

From (1)–(5), the following equation can be derived:

$$U_{Bi} - i_{Bi} \cdot R_{Ei} = u_0 \quad (6)$$

where

$$R_{Ei} = R_{BLi} + \frac{1-d}{d} \cdot R_{Cfi} + \frac{1}{d} \cdot (R_i + R_{oni}). \quad (7)$$

In Fig. 2, the transformer is equivalent to an ideal transformer with inductance  $L_m$ . From the energy conservation law, we can get

$$i_{T1}u_0 + i_{T2}u_0 + \dots + i_{Tn}u_0 = 0. \quad (8)$$

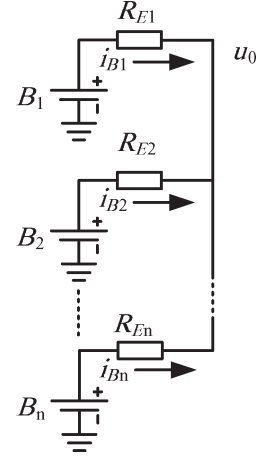


Fig. 3. Equivalent circuit model of the balance circuit, neglecting parasitic parameters, named as Model B.

By substituting  $i_{Ti}$  using  $i_{Ri}$ , we obtain

$$i_{R1} + i_{R2} + \dots + i_{Rn} = i_{Lm}. \quad (9)$$

From (4) and (9), the following equation can be obtained:

$$i_{B1} + i_{B2} + \dots + i_{Bn} = \overline{i_{Lm}} \approx 0. \quad (10)$$

Equations (6), (7), and (10) are equivalent to the circuit model shown in Fig. 3. It is simple because all the battery cells are just connected together with a resistor, so all the cell voltage will be equalized. The resistance can be controlled by MOSFET turn-on duty ratio using (7); thus, the balance current can be controlled. The asymmetry of battery connection, such as wire length, battery internal resistance, capacitor equivalent series resistance, MOSFET on-resistance, and output current limit resistance, will make  $R_{Ei}$  different. However, this only affects the balance current, not the final balance voltage. So, the circuit can achieve ideal balance voltage as long as the multiwinding transformer has sufficient symmetry.

## B. Magnetization Current Reset and Soft Switching

When the MOSFETs are on, the balance function works like a forward converter. In this application, a capacitor  $C_{si}$  is applied for each balance unit to form a resonant circuit with the main transformer inductance. The reset of magnetization current, as well as soft switching of the MOSFETs, can be achieved by the resonance.

Assume that all the MOSFETs are turned off at  $t = t_0$ . For each cell balance circuit, we have

$$\frac{1}{C_{si}} \cdot \int_0^t i_{Ri} \cdot dt + u_{Csi}(0) - i_{Ri} \cdot (R_{si} + R_i) = u_0 = L_m \cdot \frac{di_{Lm}}{dt}. \quad (11)$$

In the balance circuit design,  $R_i$  is normally less than  $0.1 \Omega$ .  $R_{si}$  is used to damp the oscillation caused by transformer leakage inductance and is about  $1 \Omega$ . The total magnetization current is less than  $0.5 \text{ A}$ . For each cell, current  $i_{Ri}$  is part of  $i_{Lm}$  and is much smaller than  $0.5 \text{ A}$ . So, in (11), the voltage

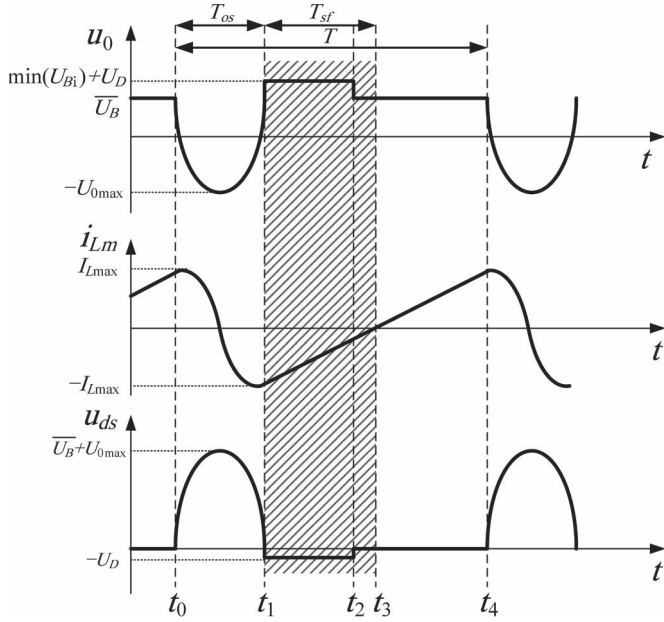


Fig. 4. Typical waveforms in one switching period.

drop on-resistances  $R_{si}$  and  $R_i$  can be neglected. Substituting  $i$  by  $1 \sim n$  and summing them up, a second-order equation is obtained to describe the resonant stage

$$L_m \cdot C_s \cdot u_0'' + u_0 = 0 \quad (12)$$

where

$$C_s = \sum_{i=1}^n C_{si}. \quad (13)$$

When the MOSFETs are on, from Fig. 3, we can get the voltage on each winding, which is the average voltage of all battery cells. So, when the MOSFETs are turned off, the resonance begins with initial condition

$$u_0(0) = \overline{U_B}. \quad (14)$$

From (12) and (13), we can see that the main transformer inductance resonates with capacitor  $C_s$ . Combining with Fig. 3, the following events occur as shown in Fig. 4. Here,  $T$  is the switching period,  $T_{os}$  is the  $LC$  oscillation period, and  $T_{sf}$  is the soft-switching time window. First, at  $t_0$ , all the MOSFETs are turned off. The magnetization current  $i_{Lm}$  discharges  $C_s$ , so  $u_0$  decreases from  $\overline{U_B}$ . Because of the  $LC$  resonance,  $C_s$  can be charged reversely to a negative high voltage, and this high voltage can shorten  $i_{Lm}$  reset time. When  $i_{Lm} = 0$ , capacitor  $C_s$  has the highest negative voltage. Then,  $i_{Lm}$  is reversely charged by  $C_s$ . When  $V_{C_s} = 0$ ,  $i_{Lm}$  has the highest negative current. After that,  $i_{Lm}$  will charge  $C_s$  again, so  $u_0$  increases. At time  $t_1$ ,  $u_0 = \min(U_{Bi}) + U_D$ , where  $U_D$  is the MOSFET body diode voltage drop, and the diode of MOSFET connected to the lowest voltage cell will turn on.  $u_0$  is clamped to  $\min(U_{Bi}) + U_d$ . At this time, the drain-source voltage on all of the MOSFETs will be equal to or less than the voltage drop of the body diode. In  $t_1 \sim t_2$ , the magnetizing current flows into the lowest voltage cell. This helps the balance. At

time  $t_2$ , all of the MOSFETs are turned on with a very low voltage, so the switching loss can be minimized. In Fig. 4, the soft-switching area is marked with shadow. After  $t_1$ ,  $u_{ds}$  can maintain nearly zero as long as  $i_{Lm}$  is negative. However, if the MOSFETs are not turned on before  $t_3$ , the diode will be turned off, and  $C_s$  will resonate with  $i_{Lm}$  again with an initial condition  $u_0(t_3) = \min(U_{Bi}) + U_D$ ,  $i_{Lm}(t_3) = 0$ .

Aside from (14), we need  $u_0'(0)$  to solve (12). From Fig. 4, we can obtain the following equation:

$$u_0'(0) = -\frac{1}{C_s} i_{Lm}(0) \approx -\frac{\overline{U_B} \cdot (T - T_{os})}{2 \cdot L_m \cdot C_s}. \quad (15)$$

In (15), the relation of  $T$  and  $T_{os}$  is not given, so we need one more equation. Here, we introduce a parameter  $\lambda$  (always  $> 1$ ), and the definition of  $\lambda$  is

$$\lambda = \frac{U_{0max}}{\overline{U_B}}. \quad (16)$$

From Fig. 4, it can be seen that the MOSFET drain-source voltage is  $(\lambda + 1) \cdot \overline{U_B}$ , and  $\lambda$  is a design parameter. It should make full utilization of the MOSFET voltage rating to decrease magnetization current reset time. So, a larger duty ratio can be applied to get higher balance current. From (12)–(16), we can get

$$\begin{cases} T = (2\sqrt{\lambda^2 - 1} + 2 \sin^{-1} \frac{1}{\lambda} + \pi) \cdot \sqrt{L_m C_s} \\ T_{os} = (2 \sin^{-1} \frac{1}{\lambda} + \pi) \cdot \sqrt{L_m C_s} \\ T_{sf} = \sqrt{\lambda^2 - 1} \cdot \sqrt{L_m C_s}. \end{cases} \quad (17)$$

From (17), we can calculate the range of MOSFET turn-on duty ratio in soft-switching condition

$$\begin{cases} d_{min} = \frac{T - T_{os} - T_{sf}}{T} = \frac{\sqrt{\lambda^2 - 1}}{2\sqrt{\lambda^2 - 1} + 2 \sin^{-1} \frac{1}{\lambda} + \pi} \\ d_{max} = \frac{T - T_{os}}{T} = \frac{2\sqrt{\lambda^2 - 1}}{2\sqrt{\lambda^2 - 1} + 2 \sin^{-1} \frac{1}{\lambda} + \pi}. \end{cases} \quad (18)$$

## IV. SIMULATION

A set of balance circuit parameters for a four-cell battery group is given in this section. Then, the equivalent circuit model in Fig. 3 is verified by simulation. The switching waveform is also given to compare with the analysis results and demonstrate the soft-switching characteristics. Lastly, the circuit is applied to two different battery groups to show the effectiveness.

### A. Circuit Parameters

In most lithium-ion battery applications, the voltage of each cell is less than 4.2 V. For low-voltage MOSFET, 30 V is a commonly seen breakdown drain-to-source voltage. So, we choose 5 for the  $\lambda$  value. The maximum  $u_{ds}$  will be 25 V. Considering the gate driving loss, and transformer and inductor volume, we choose 100 kHz for the switching frequency. To increase the balance current, no external resistor is added to limit the balance current. The resistance value in (7) is evaluated according to the wire resistance and parasitic resistance. The circuit parameters are listed in Table I.

TABLE I  
BALANCE CIRCUIT PARAMETERS

Symbol	Value	Comment
$T$	10 $\mu$ s	MOSFET switching period
$U_{Bmax}$	4.2V	Maximum voltage of each battery cell
$U_{dsmax}$	25 V	Maximum MOSFET drain-source voltage
$R_{BLi}$	0.1 ohm	Overall line resistance on battery side
$L_{fi}$	2.7 $\mu$ H	Output filter inductance
$C_{fi}$	220 $\mu$ F	Output filter capacitor
$R_{Cfi}$	0.04 ohm	ESR of $C_{fi}$
$R_{oni}$	27 mohm	IRLML0030 @ ( $I_{ds} = 5.2A, V_{gs} = 6V, 25^\circ C$ )
$C_{si}$	4.7 nF	Snubber capacitor for each cell
$R_{si}$	1 ohm	Damping resistor for each cell
$R_i$	0.05ohm	Transformer winding resistance
$L_m$	30 $\mu$ H	Transformer main inductance
$d_{min}$	0.368	Minimum on duty ratio in soft-switch range
$d_{max}$	0.736	Maximum on duty ratio in soft-switch range

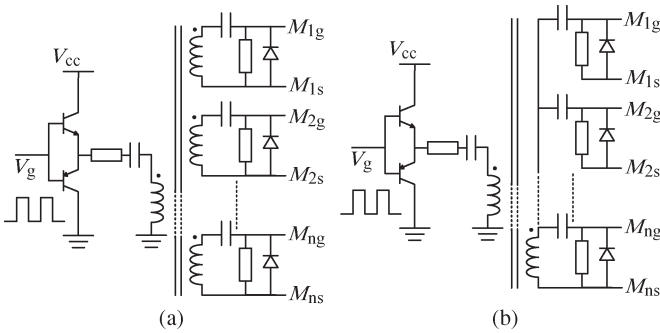


Fig. 5. MOSFET driving circuits. (a) Multiwinding transformer configuration. (b) Dual-winding transformer configuration.

TABLE II  
SIMULATION PARAMETERS

	Cell #	Battery Voltage	Other parameters
Case1	1	3.5V	The same as in Table I.
	2	3.3V	The same as in Table I.
	3	3.3V	The same as in Table I.
	4	3.3V	The same as in Table I.
Case2	1	3.5V	R, L, C increase 50%
	2	3.4V	The same as in Table I.
	3	3.3V	The same as in Table I.
	4	3.2V	The same as in Table I.

### B. Simulation of Balance Function

LTspice software is used to simulate circuit Model A shown in Fig. 2. Another circuit shown in Fig. 5(a) is used for the driving of all MOSFETs, and there is only one control signal. Fig. 5(b) can be used as the driving circuit as an alternative, so the driving transformer can be simplified. Circuit Model B in Fig. 3 is very simple, so the balance current is calculated by hand. Two cases are simulated by both models with the parameters in Table II. Fig. 6(a) shows the balance current for Case 1, and Fig. 6(b) shows the balance current under Case 2. It shows the balance current under asymmetrical parameters. Higher voltage cells are discharged, and lower voltage cells are charged. The balance function works well. Also, the results of the two models agree very well. At high duty ratio, there is almost no difference between the two models. While in lower duty ratio, the magnetization current will flow into the lower voltage cells during time  $t_1 \sim t_2$  shown in Fig. 4. This is not

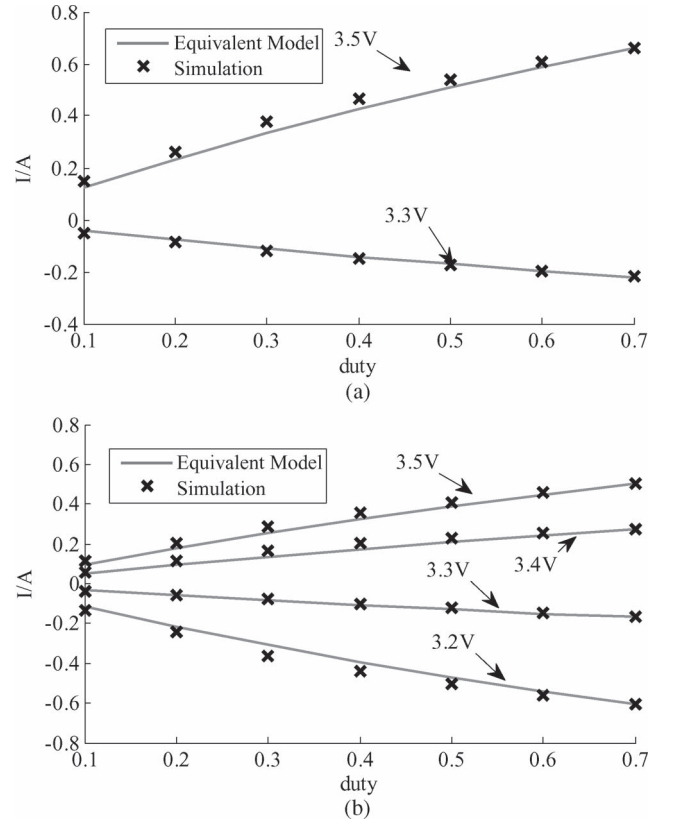


Fig. 6. Simulated balance current. (a) Under symmetrical parameters; (b) under asymmetrical parameters.

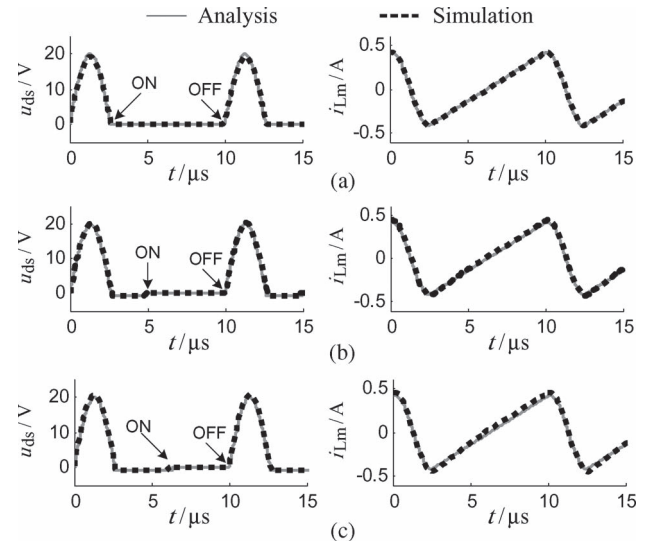


Fig. 7. Waveforms in soft-switching range. (a) duty = 0.736. (b) duty = 0.5. (c) duty = 0.368.

considered in model B. So, there is a small difference of the balance current at lower duty ratio.

### C. Switching Waveforms

Fig. 7 shows the drain-source voltage of MOSFET  $M_1$  and the magnetizing current of multiwinding transformer under soft-switching operation range for Case 1. Both analytical and simulation waveforms are given. The two results are very close.

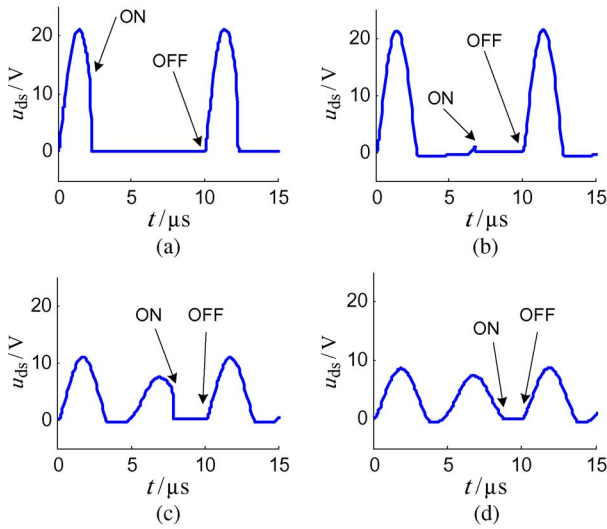


Fig. 8. Waveforms out of soft-switching range. (a) duty = 0.8. (b) duty = 0.3. (c) duty = 0.2. (d) duty = 0.1.

Only in low duty ratio situation, the magnetizing current has slight difference. This is because, in the analytical model, the contribution from diode voltage drop is not considered. When the on duty ratio of MOSFETs is small, the diode is on for a longer period of time, and this brings some error in the magnetizing current calculation. The  $u_{ds}$  waveform shows that the MOSFET is turned on and off at zero voltage. Hence, soft switching is achieved.

When the duty ratio is more than 0.736, the MOSFET will be turned off before  $u_{ds}$  resonates to zero. If the duty ratio is less than 0.368,  $u_{ds}$  will go above zero again. Soft-switching condition may be lost under these duty ratios. The simulation waveforms are shown in Fig. 8.

#### D. Balancing Performance for Four-Cell Battery Strings

In this part, the balance circuit is applied to two battery strings which are composed of valence IFR-18650EC lithium-ion cells. The cell nominal capacity is 1.35 Ah. One string has 12 cells in series; the other string has 12 rows in series with 10 cells in parallel for each row. A dynamic battery model [21] based on the parameters extracted from the datasheet is selected to simulate the battery string characteristics. The balance circuit is evaluated when the battery strings are under both charging and discharging stages. The simulation time lasts several hours to get the charging and discharging cycles. We use equivalent circuit model in Fig. 3 to reduce the computer running time. Two scenarios are studied here.

S-I. All the cells or rows have the same capacity, but the initial SOC is different. One starts with 30% SOC, and the others start with 20% SOC.

S-II. All the cells or rows have the same initial SOC of 20%, but the capacity is different. One has 95% nominal capacity, and the others have 100% nominal capacity.

For both S-I and S-II, we first charge the battery pack to full using the following charging method. First, we charge the pack by  $C/2$  current. When the highest voltage cell reaches 3.65 V, we reduce the charging current to keep the highest cell voltage

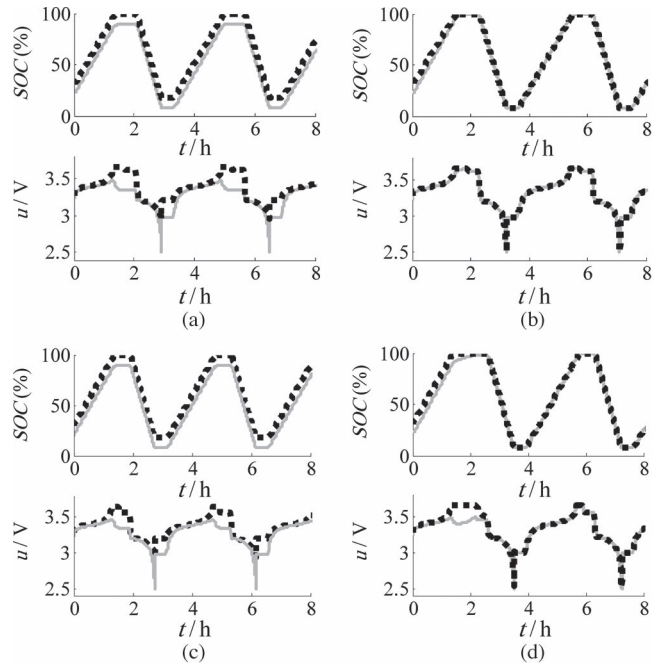


Fig. 9. Simulation of balance circuit for Case S-I, charging performance. (a) 1.35-Ah pack without balance. (b) 1.35-Ah pack with balance. (c) 13.5-Ah pack without balance. (d) 13.5-Ah pack with balance.

constant. When the charging current is less than  $C/20$ , we stop charging because the highest voltage cell is already fully charged. After the battery pack is fully charged, we discharge it by constant current until one cell reaches the cutoff voltage of 2.5 V. Between every charging and discharging stages, the battery packs are set to idle for 1500 s to observe the open-circuit voltage. The battery characteristics are simulated with and without balance circuit in this procedure.

For S-I, battery strings are discharged by  $1C$  current. The simulation results are shown in Fig. 9. The dashed line represents the different cell. For the 1.35-Ah battery string, the voltage and SOC are equalized within one charging and discharging cycle. For the larger capacity string, the 13.5-Ah battery string, it is balanced within two cycles. For the same voltage difference, the balance current is the same. For the larger capacity battery string, it takes longer time to get balanced.

For S-II, the simulation results are shown in Fig. 10. With balance circuit, more energy can be discharged from the batteries. For the smaller capacity string, the improvement of discharged energy is nearly 5%, and almost all of the capacity of each cell can be fully utilized. For the larger capacity string, the improvement with lower discharging current is bigger than that with higher discharging current. The improvement decreases from about 4.5% to 1.5% when the discharging current increases from  $C/2$  to  $2C$ . This is because the parasitic resistance in the simulated circuit is not optimized for larger capacity battery pack.

Nowadays, the MOSFET turn-on resistance can be as low as 1 m $\Omega$ . By carefully designing the transformer, we can use less turns for each winding to reduce the copper resistance. By locating the balance circuit close to the battery terminals, the total resistance could be reduced to 5–10 m $\Omega$ , so the balance current could be increased by ten times (about 5–10 A for 0.1-V

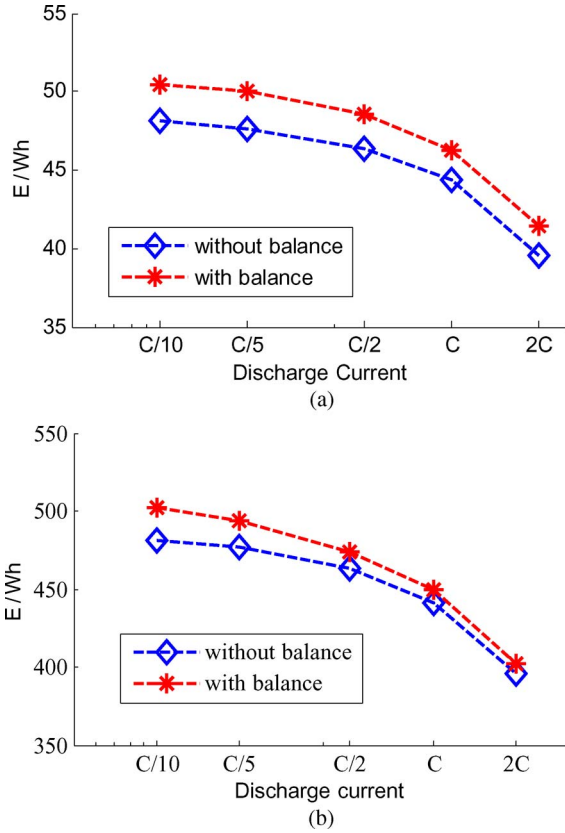


Fig. 10. Discharging energy under different currents for Case S-II. (a) Available energy from the 1.35-Ah battery string. (b) Available energy from the 13.5-Ah battery string.

voltage difference) to support fast balancing of large-capacity battery packs.

## V. EXPERIMENTAL RESULTS

To validate the analysis and simulation results, a balance circuit board for a four-cell battery group is designed according to the parameters listed in Table I.

Twisted multi-strand magnet copper wire is used to make the multiwinding transformer. The twist process makes the windings coupling tight and a high spatial symmetry is achieved. Isolation between different windings is attained by the wire insulation layer. In real production, the isolation stage should be strengthened for reliability.

For each winding, five strands of magnet wire with a copper diameter of AWG30 is chosen for the transformer to eliminate skin effect. The wire can carry 2.5-A current with about 25 °C temperature rise in still-air condition. The transformer turn ratios are measured by BK precision 4040 A signal generator and Fluke 87III True RMS multimeter. The asymmetry is less than 0.5%, and the coupling coefficient is greater than 0.999. The main inductance is 33  $\mu$ H, and the leakage inductance is less than 20 nH.

To test the balance circuit, a 0.02- $\Omega$  current shunt and TI INA282 current shunt monitor is added to each cell to measure the balance current. The balance circuit is monitored and controlled by DSpace DS1104 board. All the battery cell voltage and current signals are sampled. The MOSFET turn-on duty

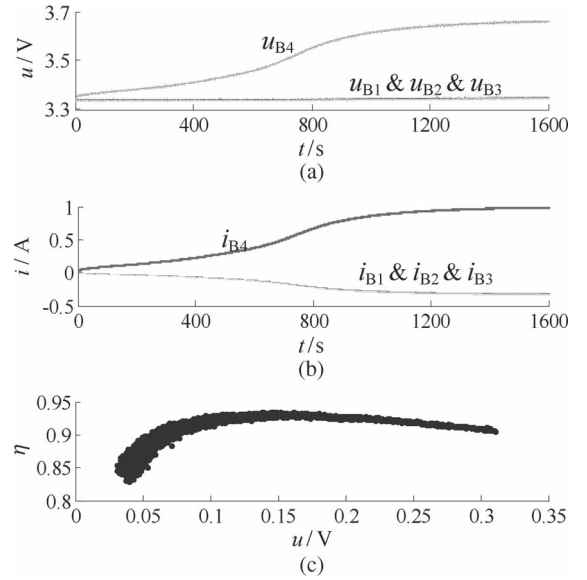


Fig. 11. Experiment results of balance current. (a) Voltage of each cell. (b) Current of each cell. (c) Efficiency versus voltage difference.

ratio is controlled by one of the DS1104 pulsewidth-modulation signals.

### A. Balance Function Test

To demonstrate the balance function, one battery cell (B4) was charged to a higher voltage (3.65 V) than the other three battery cells (3.35 V). Fig. 11(a) and (b) shows the voltage and current of each cell, respectively, when the balance circuit is turned on. To generate the largest balance current, the duty ratio was set to 0.7. The current flows out of B4 and into the other three lower voltage cells. Also, the balance efficiency is calculated by (19), and the efficiency versus voltage difference is shown in Fig. 11(c). The balance circuit has more than 85% efficiency when the voltage difference is from 0.05 to 0.3 V with the highest efficiency of up to 93%. This means that, in the whole balancing period, the circuit will have high efficiency

$$\eta = \frac{\text{abs}(u_{B1} \cdot i_{B1} + u_{B2} \cdot i_{B2} + u_{B3} \cdot i_{B3})}{u_{B4} \cdot i_{B4} + P_{\text{drv}}} \quad (19)$$

where  $P_{\text{drv}}$  is the power loss of the driver circuit, which is about 40 mW.

In real applications, it is better to know the balance current of each cell so that the BMS can get accurate current information. However, using a current sensor for each cell will bring extra cost and more complexity. Since we have the balance model in Fig. 3, it is easy to get a balance current estimation from the cell voltage. Fig. 12 shows the balance current estimation results under different voltages and duty ratios. The estimated values agree with the measurements very well.

Fig. 13 shows the MOSFET drain-source and gate-source voltages under a duty ratio of 0.1–0.7. Soft switching is achieved at 0.4–0.7. The lithium-ion battery cell voltage difference in normal operation is less than 0.5 V. Most of the time, the circuit works at 0.7 duty ratio to get a higher balance current.

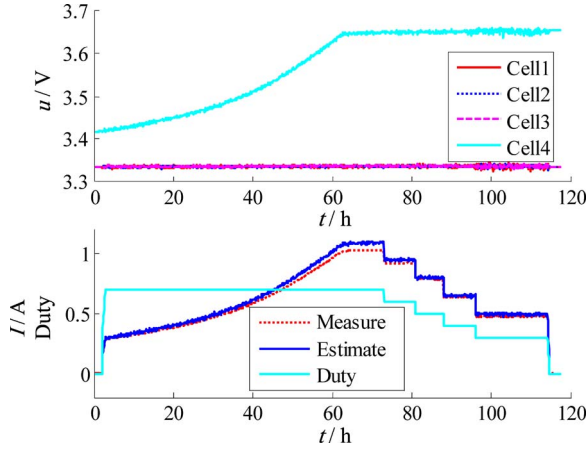


Fig. 12. Estimated balance current in comparison to measured balance current.

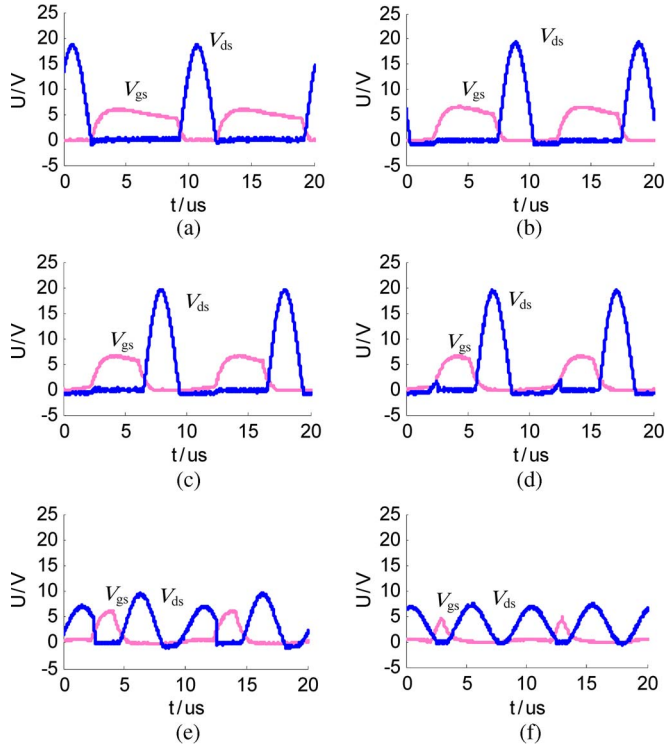


Fig. 13. Experimental waveforms of MOSFET switching voltage. (a) duty = 0.7. (b) duty = 0.5. (c) duty = 0.4. (d) duty = 0.3. (e) duty = 0.2. (f) duty = 0.1.

TABLE III  
ACTUAL CAPACITY OF EACH CELL

	Cell1	Cell2	Cell3	Cell4
Pack1	1.15 Ah	1.06 Ah	0.84 Ah	1.10 Ah
Pack2	26.1 Ah	26.2 Ah	25.8 Ah	26.5 Ah

**B. Balance Performance for Series-Connected Battery Strings**

Two battery strings composed of valence IFR-18650EC have been tested with and without the balance circuit. The nominal capacities of battery String 1 and String 2 are 1.35 and 32.4 Ah, respectively. The actual capacities are measured and listed in Table III. For smaller capacity String 1, the balance ability of making more utilization of each cell’s capacity is demonstrated. The four cells are selected with big difference to show the

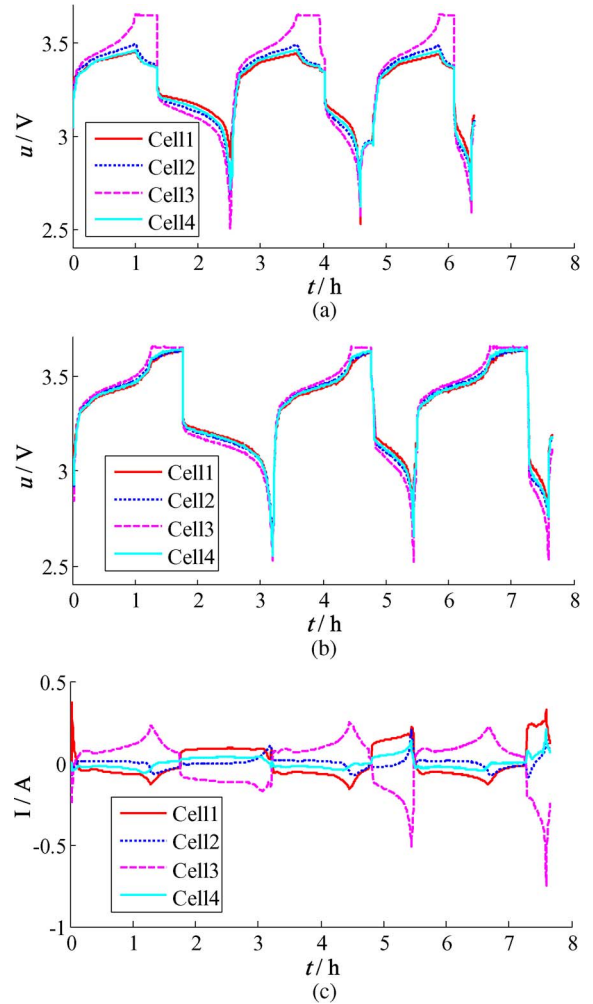


Fig. 14. Cycles without and with balance for pack1. (a) Cell voltages without balance. (b) Cell voltages with balance. (c) Balance current for each cell.

balance effect under different capacities. For larger capacity String 2, the balance ability of making cell voltage equalization is demonstrated.

For String 1, we first discharged each cell individually to empty, so the initial status is balanced. Then, we charged and discharged the battery pack for three cycles. The charging strategy was the same as mentioned in the simulation. The discharging currents were  $C/2$ ,  $1C$ , and  $2C$  for each cycle. The battery voltages are shown in Fig. 14. When the cell capacities are unequal, even with the initial voltage balanced, the cell voltage can have a big difference without the balance circuit. When the balance circuit is applied, the voltage difference becomes much smaller. With the balance circuit, more energy can be charged into the battery string at the charging stage. When discharging, weaker cells are always charged by other cells. So, the battery string capacity can be increased. Table IV shows the improvement obtained by the balance circuit.

For String 2, we first discharged each cell individually to empty. After that, we charged 2.6 Ah into cell4 separately to purposely make the initial SOC different. Then, we charged and discharged the battery pack for several cycles. The charging current is 20 A, and the discharging current is 24 A. In cycle 0, the balance circuit is off. In cycles 1–3, the balance circuit

TABLE IV  
DISCHARGED ENERGY FOR PACK1

	Without balance	With balance	Improvement
Cycle 1	10.53Wh	12.94Wh	22.89%
Cycle 2	10.05Wh	12.23Wh	21.69%
Cycle 3	9.18Wh	10.86Wh	18.3%

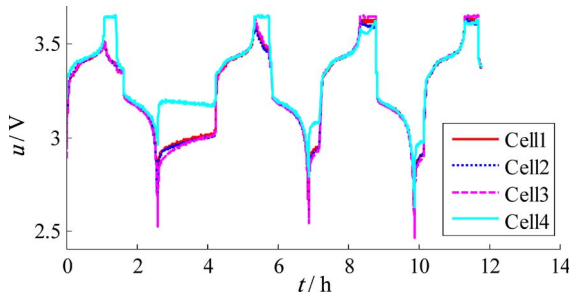


Fig. 15. Cell voltages with balance for pack2.

TABLE V  
DISCHARGED ENERGY FOR PACK2

	Energy	Improvement
Cycle 0	286.5Wh	N/A
Cycle 1	295.4Wh	3.1%
Cycle 2	315.0Wh	6.8%
Cycle 3	319.6Wh	1.6%

is on. The cell voltages are shown in Fig. 15. It can be seen that the voltages are equalized. Between cycles 1 and 2, there is an idle time for about an hour. During this idle time, the SOC is different at low SOC status. The voltage difference is significant, so higher balance current can be achieved. With this idle time, cycle 2 had about 6% capacity recovery. However, without the idle time, the balance effect is also obvious. Cycle 1 recovered about 3% of cycle 0's capacity, and cycle 3 recovered about 1.5%. The discharged energy for each cycle is listed in Table V.

## VI. CONCLUSION

In this paper, a battery-balancing circuit using multiwinding transformer has been proposed. The equivalent circuit is built and verified, and the soft-switching condition is analyzed. The circuit can balance a number of battery cells using only one control signal. Energy transfers directly from higher voltage cells to lower voltage cells, so high efficiency can be obtained. As long as the multiwinding transformer is sufficiently symmetrical, the circuit can achieve favorable balance voltage regardless of any other components' asymmetry. Simulation and experiments showed the effectiveness of the circuit.

Although the testing was carried out for four-cell battery strings, it can be easily extended to multiple-cell packs. However, the authors believe that building a multiwinding transformer with high symmetry will become more difficult when the number of windings exceeds 12. Hence, it is preferable that battery cells are balanced in groups. An additional balance circuit can be used to balance among the groups.

A 12-cell balance circuit has been built and tested in the laboratory. The experiments on the 12-cell balance circuit have showed consistent results with the ones obtained for the four-cell circuit discussed in this paper.

## REFERENCES

- [1] S. T. Hung, D. C. Hopkins, and C. R. Mosling, "Extension of battery life via charge equalization control," *IEEE Trans. Ind. Electron.*, vol. 40, no. 1, pp. 96–104, Feb. 1993.
- [2] N. H. Kutkut, H. L. N. Wiegman, D. V. Divan, and D. W. Novotny, "Design considerations for charge equalization of an electric vehicle battery system," *IEEE Trans. Ind. Appl.*, vol. 35, no. 1, pp. 28–35, Jan./Feb. 1999.
- [3] P. A. Cassani and S. S. Williamson, "Significance of battery cell equalization and monitoring for practical commercialization of plug-in hybrid electric vehicles," in *Proc. 24th Annu. IEEE APEC*, 2009, pp. 465–471.
- [4] S. M. Lukic, C. Jian, R. C. Bansal, F. Rodriguez, and A. Emadi, "Energy storage systems for automotive applications," *IEEE Trans. Ind. Electron.*, vol. 55, no. 6, pp. 2258–2267, Jun. 2008.
- [5] M. Moody, "A high reliability battery management system," *J. Power Sources*, vol. 18, pp. 223–231, 1986.
- [6] S. W. Moore and P. J. Schneider, "A review of cell equalization methods for lithium ion and lithium polymer battery systems," presented at the SAE World Congr., Detroit, MI, 2001, Paper 2001-01-0959.
- [7] C. Pascual and P. T. Krein, "Switched capacitor system for automatic series battery equalization," in *Proc. 12th Annu. APEC*, 1997, vol. 2, pp. 848–854.
- [8] L. Yuang-Shung and C. Ming-Wang, "Intelligent control battery equalization for series connected lithium-ion battery strings," *IEEE Trans. Ind. Electron.*, vol. 52, no. 5, pp. 1297–1307, Oct. 2005.
- [9] L. Yuang-Shung and C. Guo-Tian, "Quasi-resonant zero-current-switching bidirectional converter for battery equalization applications," *IEEE Trans. Power Electron.*, vol. 21, no. 5, pp. 1213–1224, Sep. 2006.
- [10] Y.-S. Lee, C.-E. Tsai, Y.-P. Ko, and M.-W. Chen, "Charge equalization using quasi-resonant converters in battery string for medical power operated vehicle application," in *Proc. IPEC*, 2010, pp. 2722–2728.
- [11] A. C. Baughman and M. Ferdowsi, "Double-tiered switched-capacitor battery charge equalization technique," *IEEE Trans. Ind. Electron.*, vol. 55, no. 6, pp. 2277–2285, Jun. 2008.
- [12] P. A. Cassani and S. S. Williamson, "Design, testing, and validation of a simplified control scheme for a novel plug-in hybrid electric vehicle battery cell equalizer," *IEEE Trans. Ind. Electron.*, vol. 57, no. 12, pp. 3956–3962, Dec. 2010.
- [13] N. Ziling and C. Mi, "Fast battery equalization with isolated bidirectional DC-DC converter for PHEV applications," in *Proc. IEEE VPPC*, 2009, pp. 78–81.
- [14] M. Einhorn, W. Guertlschmid, T. Blochberger, R. Kumpusch, R. Permann, F. V. Conte, C. Kral, and J. Fleig, "A current equalization method for serially connected battery cells using a single power converter for each cell," *IEEE Trans. Veh. Technol.*, vol. 60, no. 9, pp. 4227–4237, Nov. 2011.
- [15] S. Hanxin, Z. Wenlong, and W. Chen, "Charge equalization using multiple winding magnetic model for lithium-ion battery string," in *Proc. APPEEC*, 2010, pp. 1–4.
- [16] S.-H. Park, K.-B. Park, H.-S. Kim, G.-W. Moon, and M.-J. Youn, "Cell-to-cell charge equalization converter using multi-winding transformer with reduced number of windings," in *Proc. IEEE 8th ICPE ECCE*, 2011, pp. 285–290.
- [17] N. H. Kutkut, D. M. Divan, and D. W. Novotny, "Charge equalization for series connected battery strings," *IEEE Trans. Ind. Appl.*, vol. 31, no. 3, pp. 562–568, May/Jun. 1995.
- [18] D. M. Divan, N. H. Kutkut, D. W. Novotny, and H. L. Wiegman, "Battery charging using a transformer with a single primary winding and plural secondary windings," U.S. Patent 5 659 237, Aug. 19, 1997.
- [19] J. Chatzakis, K. Kalaitzakis, N. C. Voulgaris, and S. N. Manias, "Designing a new generalized battery management system," *IEEE Trans. Ind. Electron.*, vol. 50, no. 5, pp. 990–999, Oct. 2003.
- [20] H.-S. Park, C.-H. Kim, K.-B. Park, G.-W. Moon, and J.-H. Lee, "Design of a charge equalizer based on battery modularization," *IEEE Trans. Veh. Technol.*, vol. 58, no. 7, pp. 3216–3223, Sep. 2009.
- [21] O. Tremblay and L.-A. Dessaint, "Experimental validation of a battery dynamic model for EV applications," *World Elect. Veh. J.*, vol. 3, 2009, [Online]. Available: <http://www.evs24.org/wevajournal/vol3/title.html>



**Siqi Li** received the B.S. and Ph.D. degrees in electrical engineering from Tsinghua University, Beijing, China, in 2004 and 2010, respectively.

He is currently a Postdoctoral Fellow with the University of Michigan, Dearborn. His research interest focuses on battery management systems and high-performance battery chargers for electric vehicles.



**Chunting Chris Mi** (S'00–A'01–M'01–SM'03–F'12) received the B.S.E.E. and M.S.E.E. degrees from Northwestern Polytechnical University, Xi'an, China, and the Ph.D. degree in electrical engineering from the University of Toronto, Toronto, ON, Canada.

He was an Electrical Engineer with General Electric Canada, Inc. He is currently with the University of Michigan, Dearborn, where he is a Professor of electrical and computer engineering and the Director of the newly established U.S. Department of Energy-

funded GATE Center for Electric Drive Transportation. He is a Guest Editor of the *International Journal of Power Electronics*, is a Member of the Editorial Board of the *International Journal of Electric and Hybrid Vehicles* and *IET Electrical Systems in Transportation*, and was an Associate Editor of the *Journal of Circuits, Systems, and Computers* (2007–2009). He has conducted extensive research and published more than 100 articles. His research interests include electric drives, power electronics, electric machines, renewable energy systems, and electrical and hybrid vehicles.

Dr. Mi was the recipient of the “Distinguished Teaching Award” and “Distinguished Research Award” of the University of Michigan. He was also a recipient of the 2007 IEEE Region 4 “Outstanding Engineer Award,” “IEEE Southeastern Michigan Section Outstanding Professional Award,” and the “SAE Environmental Excellence in Transportation (E2T) Award.” He was the Chair (2008–2009) and Vice Chair (2006–2007) of the IEEE Southeastern Michigan Section. He was the General Chair of the 5th IEEE Vehicle Power and Propulsion Conference held in Dearborn on September 6–11, 2009. He is an Associate Editor of the IEEE TRANSACTIONS ON VEHICULAR TECHNOLOGY and IEEE TRANSACTIONS ON POWER ELECTRONICS—LETTERS, and IEEE TRANSACTIONS ON INDUSTRY APPLICATIONS and a Senior Editor of the *IEEE Vehicular Technology Magazine*.



**Mengyang Zhang** (M'08) received the M.S. degree in physics from West Virginia University, Morgantown, in 1993.

He is currently a Senior Technical Specialist with Chrysler Group LLC, Auburn Hills, MI. His technical areas include power-train controls and calibrations for Chrysler hybrid electric vehicle programs, and advanced vehicle electrification technologies. He has over 16 years in research and development of automotive products, including advanced power trains, electric drive systems, and chassis systems.

He taught a short course on “Fundamentals of HEV Powertrains” for the IEEE Vehicular Technology Society in 2010.